International Journal of
INTELLIGENT SYSTEMS AND APPLICATIONS IN ENGINEERING
ISSN:2147-6799 www.ijisae.org Original Research Paper

Hyper-parameter Tuning of U-Net to Breast Pectoral Muscle Segmentation and Classification using Pre-Trained Models

M. Karthik*[1], K. Thangavel[2], K. Sasirekha[3]

Submitted: 19/01/2024 **Revised**: 28/02/2024 **Accepted**: 05/03/2024

Abstract: In medical image processing, segmentation is essential for identifying and analyzing various body sections, including organs and tumors inside of them. This can support the diagnosis and treatment planning process, perhaps saving many lives. To obtain a more precise interpretation of the image, breast pectoral muscles must be removed, among other intricate pre-processes involved in the detection of breast cancer. The most popular deep learning architectures for image segmentation are SegNet and U-Net; however, fine-tuning hyperparameters will yield more accurate results from these networks. This research work combines Particle Swarm Optimization with Grey Wolf Optimization to address issues with the U-Net's hyper-parameter tuning for the excision of the breast pectoral muscle. The epoch cycles, learning ratio, Dropout Ratio, number of kernels, and activation function—all of which are hyper-parameters of the U-Net network are optimized. In comparison to traditional U-Net, U-Net with Grey Wolf, and U-Net with PSO, which show accuracies of 77.19%, 84.76%, and 89.13%, respectively, the suggested model achieved an accuracy rate of 94.28%. After segmenting the photos, the DenseNet201, EfficientNetB5, ResNet101, and VGG19 ImageNet models are used to classify them. These models produce classification accuracies of 92.01%, 97.48%, 89.56%, and 93.32%, respectively.

Keywords: *Segmentation, Breast Cancer, Pectoral Muscle, Mammogram, Hyper-parameters, Classification.*

1. Introduction

The process of splitting an image into several segments that are highly linked with its Region of Interest (RoI) area is known as image segmentation [1, 2]. The prime objective of segmenting medical images is to meaningfully characterize the raw image so that the target area may be located and the anatomy analysed to help determine the medication dose and make decisions before treatment planning. In recent decades, there has been a growing requirement for Artificial Intelligence (AI) based systems to execute AI-based segmentation tasks because of the rapid increase in tumors among people and the scarcity of experts in medical imaging science [3]. Due to their improved and fully automated performance, deep learning techniques have supplanted traditional machine learning (ML) based algorithms in recent years. Traditional segmentation methods on images, like region-centric, threshold-centric, and edge-centric approaches, have several shortcomings, including over-segmentation and high noise sensitivity [4,5]. To overcome these problems, Deep Learning networks have been utilised in recent years to create more performant photo segmentation models. Semantic, instance and panoptic segmentation are the three broad categories into which Deep Learning-based picture segmentation falls [6]. For pixels, semantic segmentation is another variant of the classification task. This segmentation method gives each pixel in the image to a class that belongs to [7]. Segmentation based on instances of objects is used to locate and identify every object of interest in the given image, is an instance segmentation [8]. The segmentation method, which is novel in this field, separates each instance of the area in the image and finds its distinctiveness by combining the properties of semantic and instance segmentation methods [9]. Convolution-based networks [10], encoder-decoder-based networks [11], regional CNN-based networks [12], and Deep Lab-based networks [13] are just a few of the deep-learning-oriented segmentation networks under development. Of them, networks based on encoder-decoders yielded the best results, especially when it came to tasks involving the segmentation of medical images [14, 15]. One of the encoder-decoder-based segmentation algorithms, U-Net was created and used for the first time in 2015 to handle biomedical images [16]. It is becoming increasingly popular among deep learning specialists, especially those who work with medical images. Although good performance is achieved, silent, hyper-parameters are crucial to get robust findings for optimal U-Net algorithm performance. To solve this problem, we introduced a fusion-based grey wolf particle swarm optimisation strategy to the U-Net model in this study. This technique helps the model avoid accepting the limits of monotonic optimisation methods and linear approaches to hyperparameter learning. The optimisation of the U-Net model's number of kernels, epoch cycles, learning ratio, dropout ratio, and activation functions is achieved by a combination of particle swarm

[1] *Department of Computer Science, Periyar University, Salem -636011, Tamil Nadu, India**
[2] *Department of Computer Science, Periyar University, Salem - 636011, Tamil Nadu, India*
[3] *Department of Computer Science, Periyar University, Salem - 636011, Tamil Nadu, India*
** Corresponding Author Email: mrjrkvgm@periyaruniversity.ac.in*

and grey wolf optimisation approaches. That is contrasted with independent implementations of the Grey Wolf along with Particle Swarm Optimisation techniques. Lastly, the ImageNet models DenseNet201, EfficientNetB5, ResNet101, and VGG19 are used to classify the segmented images.

1.1. A Contributions

1. Novel U-Net architecture segments the New Contrast Enhanced Spectral Mammography types of images.
2. A novel U-Net is implemented to optimize both Model training and designing hyper-parameters.
3. A novel Fusion-based Gray Wolf Particle Swarm approach is proposed and segmented images are classified with various ImageNet DeepCNN models.

2. Literature Survey

Several pieces of research have been carried out on the process of segmentation of breast pectoral muscle over the past few decades. But very few of them have implied the deep learning approach; Özkan Inik and Erkan Ülker [17] developed a segmentation model that segments follicles in ovarian tissue using the CNN model with various optimization algorithms including Artificial Bee Colony optimizer, Grey Wolf Optimizer, Classical Genetic Algorithm, and Particle Swarm Optimizer, methods. Among all, PSO based U-Net model attained a high accuracy value of 93.79%. However, the authors optimize only the model parameters, not the hyperparameters. Mortazi, A. et. al. [18] introduced a new cyclic optimization method built upon deep learning models including U-Net, and a CNN-based DenseNet model for segmenting the cardiac MRI images and optimizing the two hyperparameters such as learning ratio and momentum rate. Qiang Geng, and Huifeng Yan [19] designed a U-Net model that improves the accuracy and efficiency of the image segmentation process consuming the krill herb technique along with a maximum intra-class variance technique and achieved a high level of accuracy of 93.1%. Kai Zhang et. al. [20] proposed a Model-Agnostic Meta-Learning based U-Net model that employs the Particle Swarm optimization technique to segment satellite images and obtained an accuracy level of 75.44%. Diwan Baskaran et.al. [21] applied a hybrid optimization method with Multi-Scale Residual Fusion Network to segment the skin cancer data and achieved an accuracy level of 93.4% with Deep Residual Network for cancer detection.

3. Proposed Methodology

Figure 1 illustrates the building blocks of the human breast, which comprises ligaments, lymph nodes, lobules, glandular tissue, ducts, and connective tissues [22]. Although they are firmly positioned beneath the breast tissue [23], pectoral muscles are not a part of the human breast and are consistently seen in breast medical imaging.

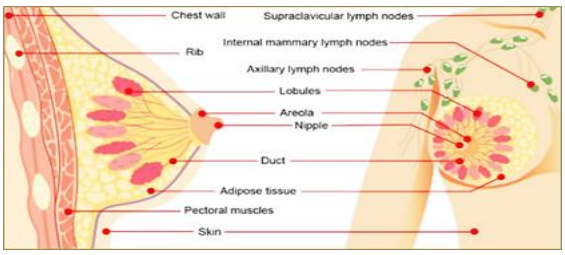

Fig. 1. Anatomy of Human Breast [24]

It is a very vital process to remove the pectoral muscle part from images for finding breast cancer using machine learning techniques particularly when images are in mammogram modality [25].

3.1. U-Net Model

U-Net, one of the deep artificial networks, and heavily employed in the segmentation of images[26]. Encoding-Decoding centered U-Net network is a kind of semantic deep neural network for the segmentation process that consists of two identical computational fragments such as down sampling and up sampling [27]. The structure of suggested U-Net network is presented in Figure. 2.

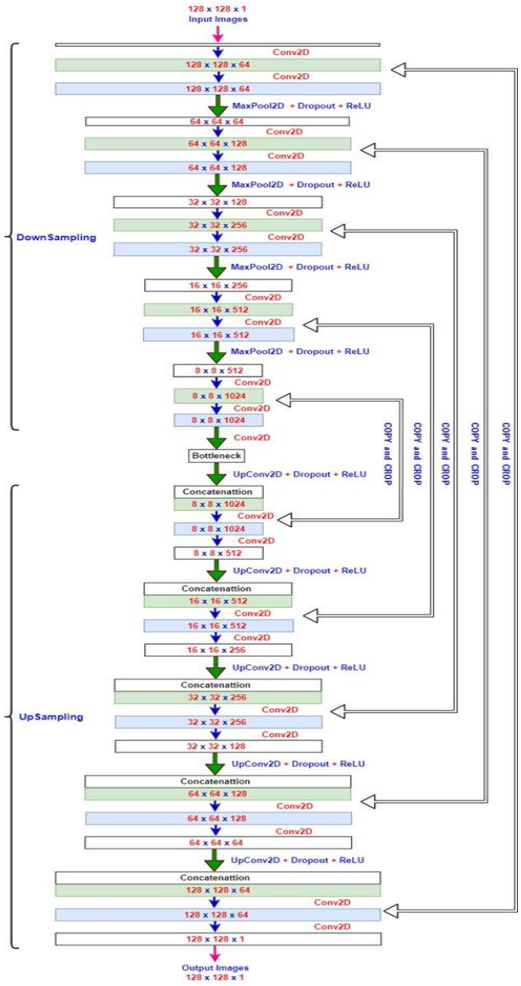

Fig. 2. The architecture of the proposed U-Net Model

The design of the suggested U-Net consists of two parts with the bottleneck portion being a down sampling part that performs a down sampling operation and an up sampling portion part performs an up sampling process on given input images. Each set of the down sampling layer consists of two convolution layers, a max-pooling layer, and a dropout layer along with an activation function. This portion is typical to utilize traditional image classification networks without the fully connected layer. The original input image is subjected to a convolution kernel pooling operation, which can provide contextual semantic information to address the classification issue in the image segmentation process [28]. Correspondingly, from the bottleneck part to the bottom of the model is an upsampling portion which is symmetrical to the down sampling portion. Each set of a layer in the upsampling portion consists of two convolution layers that perform upscaling of latent features of images and maintain (copy) the same dimensions of the image attuned in the down sampling portion along with concatenation (transpose) layer [29]. Also, at each upsampling level dropout layers are included for the elimination of overburdened neurons from the model which is very important to avoid the feature overlapping that kills the performance of the overall model [30].

3.2. Particle Swarm Optimization

Particle Swarm Optimization was originally published by Kennedy and Eberhart to simulate the behavior of bird grouping or fish schooling in 1995 [31]. The concept behind the PSO is simple, Birds either separate or assemble while hunting before relaxing in an available location. This is because birds move from one place to another in search of prey. But while in the hunting process, constantly there is always one bird that can smell the prey very clearly; this indicates that the bird is aware of where prey can be found and has the proper prey source communication. As they are sending and communicating messages to each other, all birds will fly at once in the right direction to the spot where food can be found and catch it very accurately. Initially, a set of K individual swarm particles is generated randomly and each swarm is denoted as Xi in D-dimensional vector space. The D-dimensional vector space like (xi1, xi2,...,xnd) is calculated based on movement speed(P)and velocity(V) of the swarm(s). Every swarm also keeps track of the best fitness level they have ever attained through the search process, together with the location where this fitness value was saved and recorded as pbest. Location and position corresponding to the global optimal fitness among all members of the swarm are rerecorded as gbest. The updation of each swarm is preserved by its velocity as denoted by Vmin, and Vmax. Finally, the mathematical modeling of PSO is shown in Equations 1 and 2.

$$v\_id\text{^}(t+1) = w \times v\_id\text{^}t + c\_1 \times r\_1 \times (pbaset\_id\text{^}t - x\_id\text{^}t) + c\_2 \times r\_2 \times (gbest\_id\text{^}t - x\_id\text{^}t) \quad (1)$$

$$x_{id}^{t+1} = x_{id}^{t} + v_{id}^{t+1} \quad (2)$$

Here, i is denoted as the maximum amount of iterations. The values of v and x are the real values generated in each iteration particularly, v_id^i is the velocity of a swarm in D dimensional space at a particular iteration t and x_id^t is the location factor of the same. w is the weight, c1, and c2 are accelerate constants. The r1 and r2 are two random numbers that are evenly distributed in the range [0, 1].

3.3. Grey Wolf Optimization

Grey Wolf Optimisation technique is a relatively recent approach to optimisation problem resolution. It was introduced by Seyedali Mirjalili et al. in 2014 to address design issues in the field of optical technology [32]. The basic structure of the GWO is derived from the hierarchical-oriented hunting behavior of the grey wolves. Wolves often fall into one of four categories according to the hunting hierarchy. Namely, they are Omega (γ), Beta (β), Delta (δ), and Alpha (α). Among the four wolves, the alpha wolf serves as a leader and assumes responsibility for daily activities such as hunting and surviving. The subordinates of an alpha wolf, known as beta wolves, give their decisions and backing support to the alpha wolf. The next location of the group is occupied by Omega, who upholds dominance in the hierarchy of the group. The remaining wolves that answer to the Omega are referred to as Delta. The mathematical model of GWO consists of four important steps, Equations illustrate the actions of surrounding, hunting, attacking, and searching the target. from 3 to 13. The alpha wolf must serve as the head of all four processes and uphold the wolf hierarchy.

$$\vec{D} = \left|\vec{C}.\vec{X}_p(t) - \vec{X}_p(t)\right| \quad (3)$$

$$\vec{X}(t+1) = \vec{X}_p(t) - \vec{A}.\vec{D} \quad (4)$$

In Equations 3 and 4, D $^{\rightarrow}$ is the encircling behavior of each wolf, X $^{\rightarrow}$ is the location parameter of each wolf. t is the factor of the current iteration, and A and C are coefficient factors. Equations 5 and 6 are shown below how the values of A and C are computed as follows.

$$\vec{A} = 2\vec{a}\,\vec{r}_1 - \vec{a} \quad (5)$$

$$\vec{C} = 2\vec{r}_2 \quad (6)$$

Here, the $\vec{a}$ it decreases its value linearly from 2 to 0 with an increase in the number of cycles, and within the interval of [0, 1], the value of random vectors $\vec{r}_1$ and $\vec{r}_2$ are selected [33]. From wolves' inherent hunting behavior, all types of wolves except omega, are positioned their best from the prey and it requires the positional adjustment for omega wolves for optimized prey encircling and hunting. But, before that, the position and distance of alpha, beta, and

delta are very crucial because omega is positioned based on these three categories of wolves. For that, Equations 7 to 9 find distance between the position of α, β, and δ.

$$\vec{D}_\alpha = \left|\vec{C}_1.\vec{X}_\alpha - \vec{X}\right| \quad (7)$$

$$\vec{D}_\beta = \left|\vec{C}_2.\vec{X}_\beta - \vec{X}\right| \quad (8)$$

$$D_\delta = \left|\vec{C}_3.\vec{X}_\delta - \vec{X}\right| \quad (9)$$

Based on Equations 7, 8, and 9, the locations of α, β, and δ are established through $\vec{X}_\alpha$, $\vec{X}_\beta$, and $\vec{X}_\delta$. $\vec{C}_1, \vec{C}_2$, and $\vec{C}_3$ are coefficient vectors that are randomly produced and $\vec{X}$ indicates the current position of consistent wolves. Also, the above equations 5 to 7, based on the locations of three dominant wolves, calculate an omega wolf's step size. Finally, the optimal place of alpha ($\vec{X}_1$), beta ($\vec{X}_2$), delta ($\vec{X}_3$) are calculated as the following vectors shown in equations 10, to 13.

$$\vec{X}_1 = \vec{X}_\alpha - \vec{C}_1.(\vec{D}_\alpha) \quad (10)$$

$$\vec{X}_2 = \vec{X}_\beta - \vec{C}_2.(\vec{D}_\beta) \quad (11)$$

$$\vec{X}_3 = \vec{X}_\delta - \vec{C}_3.(\vec{D}_\delta) \quad (12)$$

$$\vec{X}(t+1) = \frac{\vec{X}_1 + \vec{X}_2 + \vec{X}_3}{3} \quad (13)$$

From equations 10 to 13, $\vec{C}_1, \vec{C}_2$, and $\vec{C}_3$ are the final positions of the α, β, and δ wolves using random vectors, and determine the exact position of the omega wolves using the fixed placements of the other three wolf types. *t* represents the number of iterations it takes. In achieving optimal results using GWO, it is very important to attain the balance value between the random vectors $\vec{A}$ and $\vec{C}$. From the above equation 3, if the range of random values of $\vec{A}$ and $\vec{C}$ are greater than the *[1a, -1a]*, it improves the searchability known as the exploration capability of the wolves. Else, the random values of $\vec{A}$ and $\vec{C}$ is less than the range *[1a, -1a]*, it improves the exploitation (victimization) capability of the wolves [34]. Once the search process for hunting the prey, The number of cycles rises, and the value of the vector $\vec{A}$ falls linearly, eventually boosting the wolf's capacity for exploitation. However, because the value of $\vec{C}$ is produced at random throughout the optimisation process, the exploration and exploitation of the wolf may find symmetry at any time, particularly in the last stages of iterations. It can prevent the GWO algorithm from being stuck at local minima.

3.4. Fusion Grey Wolf and Particle Swarm Optimisation for Hyper-parameter Optimisation of U-Net

Particle Swarm and Grey Wolf are two highly potent, bio-inspired optimisation strategies that are successful in resolving optimisation problems involving nonlinear objective functions. PSO approach can be used to effectively fix almost all real-world issues. However, there must be a means to determine the possibility that the PSO will be trapped by the local minimum problem. In this proposed technique, based on the literature review, a more exploited and result-proven PSO optimization algorithm is fixed as the root optimization method for the novel U-Net used in this work. Naturally, PSO evades the local minima problem by changing some particles from one random position to another position in search space. But this does not always give the expected solution and there may be misleading the training of the algorithm into the erroneous path. To avoid this limitation, GWO is implemented with PSO. Instead of moving particles randomly in PSO, GWO gives regularity due to its hierarchical-based ranking of alpha, beta, and delta wolf characteristics into the random particles that may lead to the proper position in the available search space. The proposed model of the Fusion of Gray Wolf Particle Swarm Optimization (FGWPSO) is shown in the Figure. 3. By combining the GWO approach with the PSO, it is shown that the U-Net model is better for errors, and the processing time is remarkably gained with minimum epoch cycles. Moreover, without interruption of execution of both the algorithms, fusing GWO's alpha, beta, and delta particle values into PSO random particle values provides the seamless performance of the proposed model.

$$\vec{D}_\alpha = \left|C_1.\vec{X}_\alpha - w \times \vec{X}(t)\right| \quad (14)$$

$$\vec{D}_\beta = \left|C_2.\vec{X}_\beta - w \times \vec{X}(t)\right| \quad (15)$$

$$\vec{D}_\delta = \left|C_3.\vec{X}_\delta - w \times \vec{X}(t)\right| \quad (16)$$

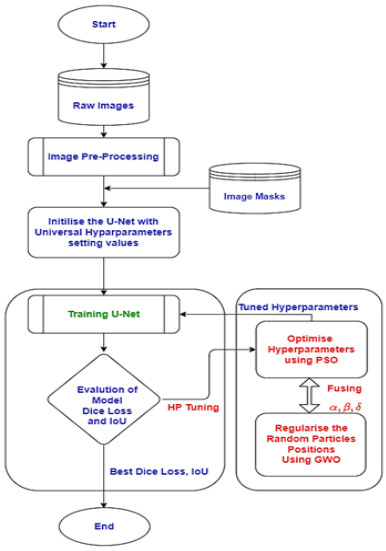

Fig. 3. The design of the proposed U-Net Model

In equations 14, 15, and 16, the position of GWO alpha, beta, and delta has been fixed with the initial inertia weight of PSO. Every iteration of GWO has been updated with PSO w value to maintain the parallelity to the PSO algorithm, and PSO has utilized ordered alpha, beta, and delta values for adjusting with random particle position in the training process. Now, the model utilises both PSO along with GWO properties to yield better accuracy with a minimum error rate and a short execution cycle. Once, the PSO's random particles are placed in proper search space, then the velocity and positions are going to be updated in PSO. Equations 17 and 18 show the update process of velocity and position.

$$v_i(t+1) = w \times [v_i t + C_1 r_1(X_1 - x_i t) + C_2 r_2(X_2 - x_i t) + C_3 r_3(X_3 - x_i t)] \quad (17)$$

$$x_i(t+1) = x_i t + v_i(t+1) \quad (18)$$

In the proposed Fusion Gray Wolf Particle Swarm optimisation method shown above in equations 17 and 18, an optimal value of the model is found using Dixen-Price Benchmark Objective Function that is shown in Equation 19.

$$f(x) = (x_i - 1)^2 + \sum_{i=2}^{d} i(2x_i^2 - x_{i-1})^2 \quad (19)$$

Dixen-Price is one of the best benchmark optimisation test functions that are continuous, differentiable, highly scalable, well suited for unimodal, non-separable, and definable on the d-dimensional space [35, 36].

4. Result and Discussion

The proposed Gray Wolf Particle Swarm Optimisation technique is implemented separately on two standard digital mammogram datasets CDD-CESM, and INBreast.

4.1. Datasets Description and Preprocessing

In Breast is a very popular but not as much of an exposed digital mammogram dataset [37], it follows both ACR and BI-RADS standards which are strictly followed in the medical imaging science for evaluating whether the patient has cancer or not from their breast images. INBreast contains a total of 410 digital mammogram images from 115 cases of women. Both the Mediolateral Oblique (MLO) and Bilateral Craniocaudal (CC) perspectives are present in the images. Since MOL photos only show the pectoral muscle area, 206 MLO images out of 410 photographs were selected for this study. A recent entrant in this sector is the CDD-CESM dataset, which contains a unique mammogram image modality called Contrast-enhanced spectral mammography [38]. The 2006 images in the CDD-CESM image data, which adheres to the BI-RADS standard, are divided into two categories: low-energy images and subtracted contrast images. From these two types, Low-energy images were only considered for this research work. Out of 1003 low-energy images that contain both CC and MLO views, 503 MLO images are taken into consideration for this research work. In any machine learning or deep learning model, a significant amount of effort into data pre-processing should be carried out to attain the proper results we expect. In this research work, all the images from both CDD-CESM and INBreast have applied two types of preprocessing methods: (i) to convert images from RGB into Grayscale mode, and (ii) histogram correction using Contrast Limited Adaptive Histogram Equalisation (CLAHE) method [39].

4.2. Hyper parameters space for optimisation

The universal value setting of hyper-parameters that are implemented by the proposed FGWPSO technique and the other three types of implementations. The range of hyper-parameters, number of kernels, Dropout Ratio, activation function, epoch cycles, and learning ratio are defined in Table 1 The activation function for the output layer in the proposed U-Net is fixed as a Sigmoid function.

Table 1 Universal Setting of Hyper-parameters Range

Hyper-parameter	Minimum Range	Maximum Range
Number of Kernels	8	512
Dropout Ratio	0.0	0.6
Activation Function	ReLU [40], LReLU [41], EReLU [42], PReLU [43], GReLU [44]	
Epochs Cycles	10	100
Learning Ratio	0.001	0.0000001

4.3. Evaluation Measures

An assessment measures to quantify the efficacy of a suggested model. The performance of the suggested U-Net model was assessed in this study using two different assessment measures: the Mean of Intersection over Union [46] and Dice Loss [45], which are presented in equations 20 and 21. The value accuracy is obtained for all four implementations but it is not included in the results because there is a high chance of class imbalance that results in accuracy not showing the original pixel label [47]. It is not recommended accuracy is suitable for segmentation problems.

$$Dice\ Loss = 1 - \frac{2TP}{2TP+FP+FN} \quad (20)$$

$$IoU = \frac{TP}{TP+FP+FN} \quad (21)$$

4.4. Result Discussion

The results from four different implementations of the various optimisation methods on the CDD-CESM dataset, and INBreast which were used for testing purposes, are described in this part. Table 2 displays the outcome of the optimal hyperparameters that were chosen, and Figures 4 and 5 display the results of the IoU and dice loss measures

of the traditional U-Net network.

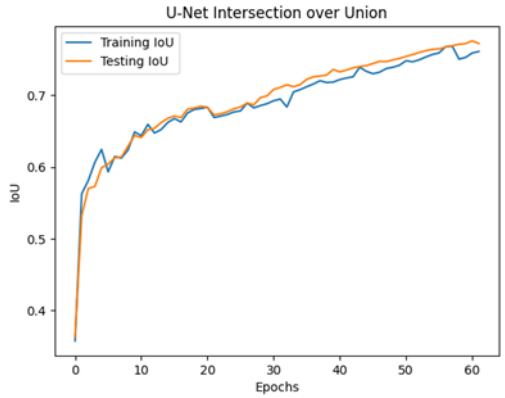

Fig. 4. IoU of the U-Net without any optimization

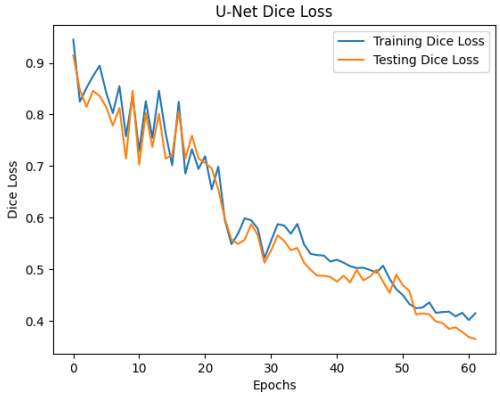

Fig. 5. Dice Loss of the U-Net without any optimization

Table 2 Best Hyper-parameter Values For U-Net Model Without Optimization Methods.

Hyper-parameter	Best Values Obtained
Number of Kernels	32, 64, 128, and 256
Dropout Ratio	0.2 to 0.4
Activation Function	ReLU
Epochs Cycles	61
Learning Ratio	0.00001

Results from Figures 4 and 5 show that the implemented U-Net model without any optimisation methods converged in 61 epochs and obtained an average IoU value of 76.08% in training and 77.19% in the testing phase. However, the model is highly unstable convergence in the Dice loss it obtained 0.41% in training and 0.37% in testing respectively. The U-Net model's implementation using the PSO optimisation approach is depicted in Figures 6 and 7, and Table 3 provides information on the optimal hyperparameters that were determined.

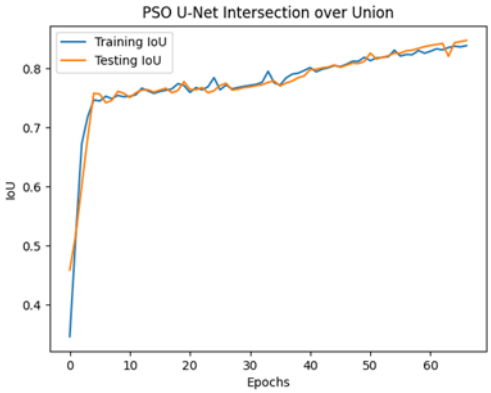

Fig. 6. IoU of U-Net with PSO Optimisation

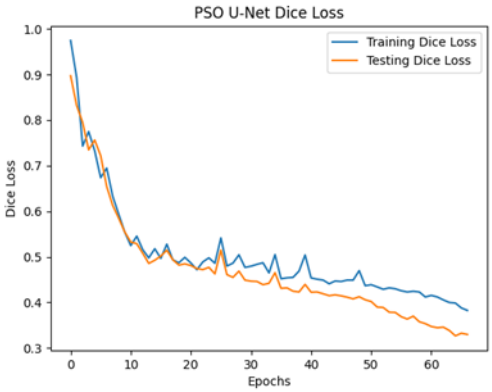

Fig. 7. Dice Loss of U-Net with PSO Optimisation

Table 3 Best Hyper-parameter Values for U-Net Model with PSO Optimisation.

Hyper-parameter	Best Values Obtained
Number of Kernels	32, 64, 128, and 256
Dropout Ratio	0.1, 0.2 and 0.4
Activation Function	LReLU
Epochs Cycles	67
Learning Ratio	0.000016

Results from Figures 5 and 5 show that the implemented U-Net model with PSO optimisation itself has toked a few additional epochs and converged in 67 epochs. The PSO U-Net model got an average IoU value that also increased significantly from 76.08% in simple U-Net to 83.87% in the training phase and 84.76% in the testing phase which is not a huge difference in train-test performance. But the model is highly convergence in the Dice loss measure, obtained 0.38% in training and 0.32% in testing has shown an acceptable performance difference. Also, the selection of the best hyper-parameters got different values. In particular, LReLU instead of ReLU is chosen as the function of activation in the PSO U-Net architecture. There are also slight variations in the learning ratio and dropout ratio.

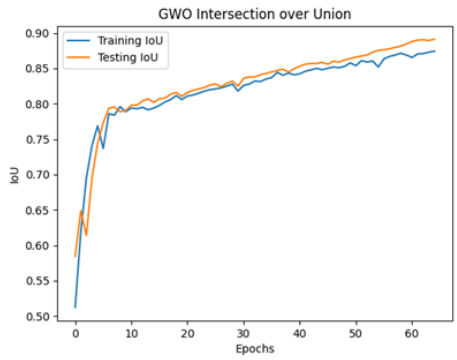

Fig. 8. IoU of U-Net model with GWO Optimisation

Fig. 9. Dice Loss for U-Net with GWO Optimisation

Table 4. Best Hyper-parameter Values For U-Net Model with GWO Optimisation.

Hyper-parameter	Best Values Obtained
Number of Kernels	32, 64, 128, and 256
Dropout Ratio	0.2 to 0.5
Activation Function	LReLU
Epochs Cycles	65
Learning Ratio	0.000012

U-Net with GWO performs better in terms of numerical values but it gives a very closer performance compared with PSO implementation. Moreover, all five hyper-parameters best values are identical compared with values obtained in the PSO implementation model. Finally, Figures 10 and 11 show the result of U-Net model with the proposed Fusion-based Gray Wolf Particle Swarm optimisation method, and Table. 5 shows the best values of all five hyper-parameters using the proposed method.

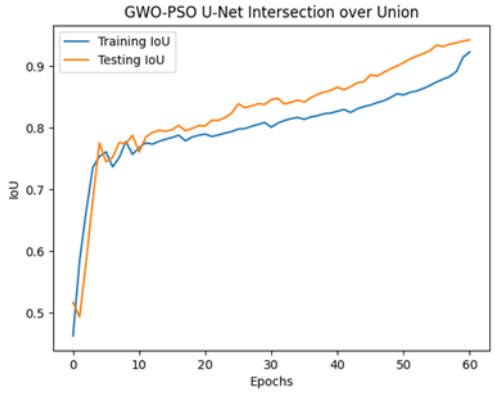

Fig. 10. IoU value of suggested U-Net

Fig. 11. Dice Loss value of the suggested U-Net

Table 5 Best Hyper-parameter Values for U-Net Model with FGWPSO Optimisation.

Hyper-parameter	Best Values Obtained
Number of Kernels	16, 32, 64, 128, 256, and 512
Dropout Ratio	0.2 to 0.5
Activation Function	ReLU
Epochs Cycles	61
Learning Ratio	0.000028

The suggested FGWPSO U-Net model yielded some unexpected results, as shown in Figures 10, 11, and Table 5. The proposed model's IoU values obtained the greatest value and also demonstrated substantial variations in performance between the training and testing stages. The suggested model attained an IoU rate of 92.33% during the training phase and 94.28% during the testing phase. This rate was sustained during the model's execution in both phases. Additionally, the suggested model attains the best Dice Loss of 0.14% during the testing phase and 0.21% during training. It demonstrates that, when compared to the three implementations, the suggested FGWPSO U-Net has the finest performance. The hyper-parameters were selected by the suggested method also getting significant value ranges.

The proposed method selects the maximum number of kernels of 512 from a minimum of 16 kernels. The values of the Dropout Ratio are selected from 0.2 up to 0.5 at different layers of the model. But, in the selection of the activation function side, the proposed method is stable with ReLU. It shows the adaptability and power of ReLu in various domain problems including medical image segmentation also. However, the learning ratio and epoch cycles are not getting very deviation compared to GWO implementation. Table. 6, and Figure 12 shows the overall difference between IoU and Dice Loss of all four U-Net model values. The results of segmented Images are shown in Figures 13 to 16.

Table 6 Comparison of All Four U-Net Models IoU and Dice Loss Values.

U-Net Models	IoU		Dice Loss	
	Training	Testing	Training	Testing
Simple U-Net	76.08 %	77.19 %	0.41 %	0.37 %
U-Net with PSO	83.87 %	84.76 %	0.38 %	0.32 %
U-Net with GWO	87.45 %	89.13 %	0.28 %	0.22 %
U-Net with FGWPSO	92.33 %	94.28 %	0.21 %	0.14 %

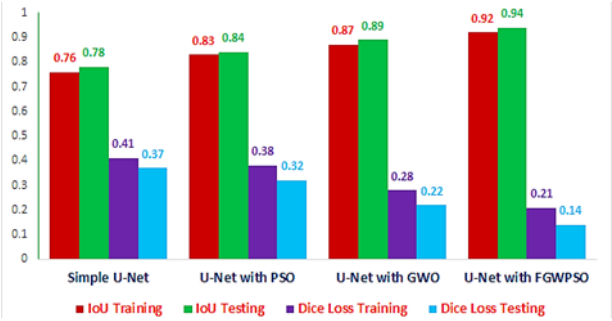

Fig. 12. The design of the proposed U-Net Model

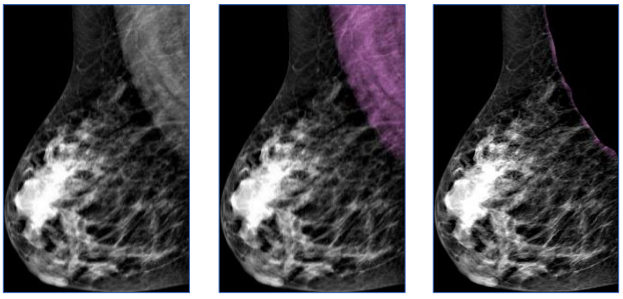

Fig. 13. (a) Raw Image (b) Pectoral Portion (c) Pectoral Predicted

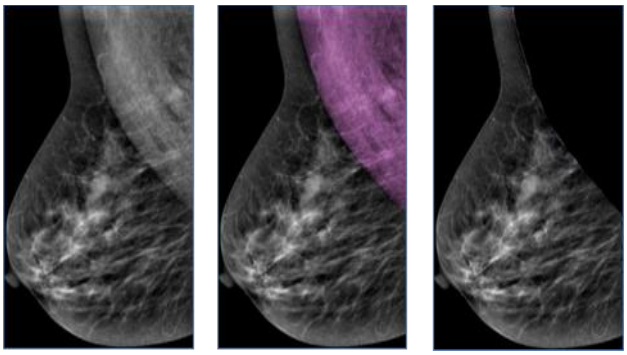

Fig. 14. (a) Raw Image (b) Pectoral Portion (c) Pectoral Predicted

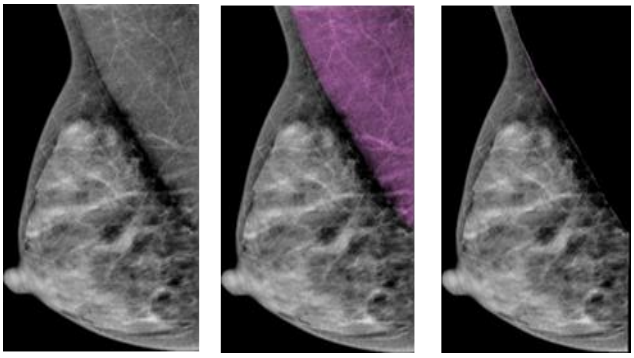

Fig. 15. (a) Raw Image (b) Pectoral Portion (c) Pectoral Predicted

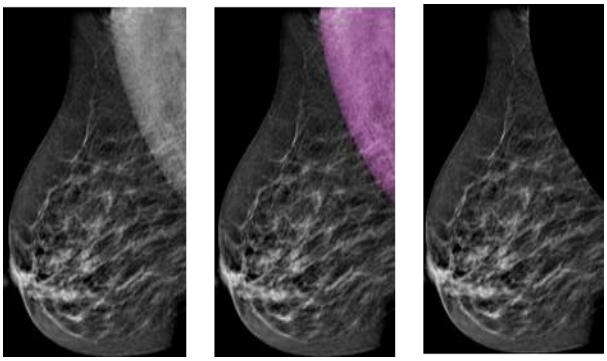

Fig. 16. (a) Raw Image (b) Pectoral Portion (c) Pectoral Predicted

The performance of segmentation process results for each of the four implementations are provided in Figures 13 through 16. The original raw input image is shown in (a) of all four figures, the ground truth annotation of the pectoral muscles region is shown in (b), and the execution of the applied U-Net model with different configurations is shown in (c).

Classification using ImageNet models. The segmented images obtained are trained with benchmark transfer learning methods DenseNet201, EfficientNetB5, ResNet101, and VGG19 to identify the breast tumor more accurately [48, 49].

Table 6 Evaluation Measures of Various Pre-Trained Models for Classification.

Model Name	Accuracy	Precision	Recall	F - Score
DenseNet201	92.01%	91.95 %	92.03 %	92.10%
EfficientNetB5	97.48%	97.37 %	97.22 %	97.29%
ResNet101	89.56%	89.97 %	89.69 %	89.43%
VGG19	93.32%	93.18 %	93.29 %	93.26%

It is evident from Table 7 and Figure 17 that the pre-trained DeepCNN Xception model outperforms the pre-trained networks examined in this work. It has been noted that the EfficientNetB5 and ResNet101 models had the highest performance and lowest recognition rates, respectively, with 99.18% and 96.21% accuracy.

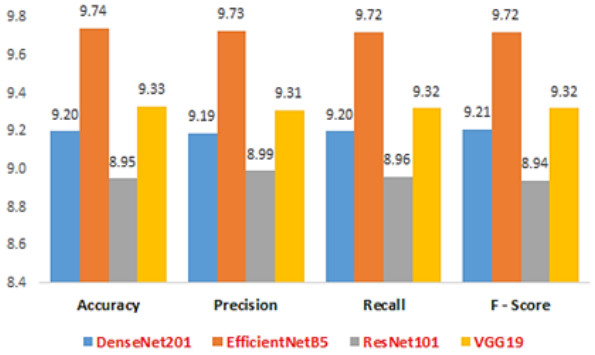

Fig. 17. Performance of Pre-Trained Models for Classification

5. Conclusion

One of the biggest issues facing the globe now is the early diagnosis of breast cancer. A digital mammogram is a well-suited type of medical imaging that is crucial for early diagnosis of breast cancer. By using the DeepCNN approach, medical report times can be significantly reduced, and patients have a better chance of survival by having a tumor found more accurately. This study suggests an improved image segmentation model that more precisely segments images by optimising the deep U-Net hyper-parameters with the combination of Particle Swarm Optimisation and Grey Wolf. Furthermore, the comprehensive testing shows that the suggested approach FGWPSO performs better than the classical architecture of U-Net, U-Net with Grey Wolf, and U-Net with PSO. To identify the breast tumor more precisely, the segmented pictures were lastly trained using ImageNet DeepCNN models, specifically DenseNet201, EfficientNetB5, ResNet101, and VGG19. These models produced accuracies of 92.01%, 97.48%, 89.56%, and 93.32%, respectively.

References

[1] Sengur, U. Budak, Y. Akbulut, M. Karabatak, and E. Tanyildizi. (2019). A survey on neutrosophic medical image segmentation. in Neutrosophic Set in Medical Image Analysis, Page 145–165.

[2] Martin Thoma. (2016). A survey of semantic segmentation, 2016, Page 1602-06541.

[3] Sengur, U. Budak, Y. Akbulut, M. Karabatak, and E. Tanyildizi. (2019). A survey on neutrosophic medical image segmentation, in Neutrosophic Set in Medical Image Analysis, Page 145–165.

[4] Tushar Jaware, Ravindra Badgujar, Jitendra Patil, Vinod Patil, Prashant Patil, Mahesh Dem-brani. ICTACT Journal on Soft Computing, Page 2651-2656.

[5] Martin Thoma, A Survey of Semantic Segmentation, arXiv: 1602.06541, https://doi.org/10.48550/arXiv.1602.06541.

[6] Alexander Kirillov, Kaiming He, Ross Girshick, Carsten Rother, Piotr Dollár, Panoptic Seg-mentation, arXiv:1801.00868, https://doi.org/10.48550/arXiv.1801.00868.

[7] Yujian Mo, Yan Wu, Xinneng Yang, Feilin Liu, Yujun Liao, Review the state-of-the-art technologies of semantic segmentation based on deep learning, Neurocomputing, Volume 493, 2022.

[8] P. Rajpurkar, J. Irvin, R. L. Ball, et al., “Deep learning for chest radiograph diagnosis: a retrospective comparison of the CheXNeXt algorithm to practicing radiologists,” PLoS Medicine, vol. 15, no. 11, Article ID e1002686, 2018.

[9] J Ramesh, K Thangavel, R Manavalan, Review on Computational Models for Prostate Seg-mentation from Ultrasound Medical Images, Journal of Clinical and Medical Images Case Reports, Volume 2, Issue 2, 2022.

[10] Fischer, P.; Dosovitskiy, A.; Brox, T. Descriptor Matching with Convolutional Neural Networks: A Comparison to SIFT. arXiv 2014, arXiv:1405.5769.

[11] Liu, Y.; Guo, Y.; Lew, S.M. On the Exploration of Convolutional Fusion Networks for Visual Recognition. In Proceedings of the MultiMedia Modeling; Springer: Cham, Switzerland, 2017; pp. 177–189.

[12] Farhana Sultana, Abu Sufian, Paramartha Dutta, Evolution of Image Segmentation using Deep Convolutional Neural Network: A Survey, arXiv:2001.04074.

[13] Yanheng Wang, Lianru Gao, Danfeng Hong, Jianjun Sha, Lian Liu, Bing Zhang, Xianhui Rong, Yonggang

Zhang, Mask DeepLab: End-to-end image segmentation for change detection in high-resolution remote sensing images, International Journal of Applied Earth Observation and Geoinformation, Volume 104, 2021.

[14] Kamrul Hasan, S.M.; Linte, C.A. A Modified U-Net Convolutional Network Featuring a Nearest-neighbor Re-sampling-based Elastic-Transformation for Brain Tissue Characterization and Segmentation. 2018 IEEE West. New York Image Signal Process. Work. WNYISPW 2018 2018, 1–5.

[15] M. Sathiya, K. Karunambiga, G. Sai Chaitanya Kumar, S. Chandra Sekaran, An Enhanced Ensemble Hybrid Deep Learning Algorithm For Improving The Accuracy In Iris Segmentation, ICTACT Journal on Image and Video Processing, Volume 13, Issue 3, 2947 – 2952.

[16] Shervin Minaee, Yuri Boykov, Fatih Porikli, Antonio Plaza, Nasser Kehtarnavaz, Demetri Terzopoulos, Image Segmentation Using Deep Learning: A Survey, arXiv:2001.05566.

[17] Inik, Ö., Ülker, E. Optimization of deep learning based segmentation method. Soft Comput 26, 3329–3344 (2022). https://doi.org/ 10.1007/s00500-021-06711-3.

[18] Mortazi, A., Cicek, V., Keles, E., & Bagci, U. (2023). Selecting the Best Optimizers for Deep Learning based Medical Image Segmentation. arXiv preprint arXiv:2302.02289.

[19] Qiang Geng, and Huifeng Yan, Image Segmentation under the Optimization Algorithm of Krill Swarm and Machine Learning, Computational Intelligence and Neuroscience, 1687-5265 (2022), Hindawi, https://doi.org/10.1155/2022/8771650.

[20] Kai Zhang, Yu Han, Jian Chen, Zichao Zhang et.al., Semantic Segmentation for Remote Sens-ing based on RGB Images and Lidar Data using Model-Agnostic Meta-Learning and Particle Swarm Optimization, IFAC-PapersOnLine, Volume 53, Issue 5, 2020, Pages 397-402. https://doi.org/10.1016/j.ifacol.2021.04.117.

[21] Diwan Baskaran, Yanda Nagamani, Suneetha Merugula & S P Premnath (2023) MSRFNet for skin lesion segmentation and deep learning with hybrid optimization for skin cancer detection, The Imaging Science Journal, 2023, DOI: 10.1080/13682199.2023. 2187518.

[22] American Cancer Society, https://www.cancer.org/cancer/breast-cancer/about/what-is-breast-cancer.html.

[23] Akram M, Iqbal M, Daniyal M, Khan AU. Awareness and current knowledge of breast cancer. Biol Res. 2017 Oct 2;50(1):33. doi: 10.1186/s40659-017-0140-9. PMID: 28969709; PMCID: PMC5625777.

[24] Dr. Mary Ling, Breast Anatomy, https://www.drmaryling.com.au /breast-anatomy.

[25] Gómez KAH, Echeverry-Correa JD, Gutiérrez ÁÁO. Automatic Pectoral Muscle Removal and Microcalcification Localization in Digital Mammograms. Healthc Inform Res. 2021 Jul;27(3):222-230. doi: 10.4258/hir.2021.27.3.222. Epub 2021 Jul 31. PMID: 34384204; PMCID: PMC8369047.

[26] Olaf Ronneberger, Philipp Fischer, Thomas Brox, U-Net: Convolutional Networks for Bio-medical Image Segmentation, arXiv:1505.04597, https://doi.org/10.48550/arXiv.1505. 04597.

[27] Hatamizadeh, D. Sengupta, and D. Terzopoulos, "End-to-end deep convolutional active contours for image segmentation," arXiv preprint arXiv:1909.13359, 2019.

[28] P. Luo, G. Wang, L. Lin, and X. Wang, "Deep dual learning for semantic image segmentation," in Proceedings of the IEEE International Conference on Computer Vision, 2017, pp. 2718–2726.

[29] Xiao-Xia Yin, Le Sun, Yuhan Fu, Ruiliang Lu, and Yanchun Zhang et.al., Recent Advances of Knowledge Discovery Assisted Clinical Diagnosis, U-Net-Based Medical Image Segmentation, Journal of Healthcare Engineering, Hindawi, 2022.

[30] Srivastava, N.; Hinton, G.; Alex, K.; Sutskever, I.; Ruslan, S. Dropout: A Simple Way to Prevent Neural Networks from Overfitting. J. Mach. Learn. Res. 2014, 299, 1929–1958.

[31] J. Kennedy and R. Eberhart, "Particle swarm optimization," Proceedings of ICNN'95 - International Conference on Neural Networks, Perth, WA, Australia, 1995, pp. 1942-1948 vol.4, doi: 10.1109/ICNN.1995.488968.

[32] Seyedali Mirjalili, Seyed Mohammad Mirjalili, Andrew Lewis, Grey Wolf Optimizer, Advances in Engineering Software, Volume 69, 2014, Pages 46-61, https://doi.org/10.1016/j. advengsoft.2013.12.007.

[33] H. Xu, X. Liu, and J. Su, "An improved grey wolf optimizer algorithm integrated with Cuck-oo Search," 2017 9th IEEE International Conference on Intelligent Data Acquisition and Advanced Computing Systems: Technology and Applications (IDAACS), Bucharest, Romania, 2017, pp. 490-493, doi: 10.1109/IDAACS.2017.8095129.

[34] Ibrahim Saiful Millah, Pei Cheng Chang, Dawit Fekadu Teshome, Ramadhani Kurniawan Subroto,

Kuo Lung Lian, Jia-Fu Lin, "An Enhanced Grey Wolf Optimization Algorithm for Photovoltaic Maximum Power Point Tracking Control Under Partial Shading Conditions", IEEE Open Journal of the Industrial Electronics Society, vol.3, pp.392-408, 2022.

[35] Shen, C., Zhang, K. Two-stage improved Grey Wolf optimization algorithm for feature selection on high-dimensional classification. Complex Intell. Syst. 8, 2769–2789 (2022). https://doi.org/10.1007/s40747-021-00452-4.

[36] Hu, P., Chen, S., Huang, H., Zhang, G., & Liu, L. (2019). Improved Alpha-Guided Grey Wolf Optimizer. IEEE Access, 7, 5421-5437.

[37] Inês C. Moreira, Igor Amaral, Inês Domingues, António Cardoso, Maria João Cardoso, Jaime S. Cardoso, INbreast: Toward a Full-field Digital Mammographic Database, Academic Radi-ology, Volume 19, Issue 2, https://doi.org/10.1016/j.acra.2011.09.014.

[38] Khaled, R., Helal, M., Alfarghaly, O. et al. Categorized contrast-enhanced mammography dataset for diagnostic and artificial intelligence research. Sci Data 9, 122 (2022). https://doi.org/10.1038/s41597-022-01238-0.

[39] S. M. Pizer, R. E. Johnston, J. P. Ericksen, B. C. Yankaskas and K. E. Muller, "Contrast-limited adaptive histogram equalization: speed and effectiveness," [1990] Proceedings of the First Conference on Visualization in Biomedical Computing, Atlanta, GA, USA, 1990, pp. 337-345, doi: 10.1109/VBC.1990.109340.

[40] Abien Fred Agarap, Deep Learning using Rectified Linear Units (ReLU), arXiv:1803.08375, https://doi.org/10.48550/arXiv.1803. 08375.

[41] Bing Xu, Naiyan Wang, Tianqi Chen, Mu Li, Empirical Evaluation of Rectified Activations in ConvolutionNetwork, arXiv:1505.00853v2 [cs.LG] 27 Nov 2015.

[42] Daeho Kim, Jinah Kim, Jaeil Kim, Elastic exponential linear units for convolutional neural networks, Neurocomputing, Volume 406, 2020.

[43] Kaiming He, Xiangyu Zhang, Shaoqing Ren, Jian Sun, Delving Deep into Rectifiers: Surpassing Human-Level Performance on ImageNet Classification, arXiv:1502.01852.

[44] Dan Hendricks, Kevin Gimpel, Gaussian Error Linear Units (GELUs), arXiv:1606.08415, https://doi.org/10.48550/arXiv.1606.08415.

[45] Carole H Sudre, Wenqi Li, Tom Vercauteren, Sébastien Ourselin, M. Jorge Cardoso, Generalised Dice overlap as a deep learning loss function for highly unbalanced segmentations, arXiv:1707.03237, https://doi.org/10.48550/arXiv.1707.03237.

[46] Dingfu Zhou, Jin Fang, Xibin Song, Chenye Guan, Junbo Yin, Yuchao Dai, Ruigang Yang, IoU Loss for 2D/3D Object Detection, arXiv: 1908.03851, https://doi.org/10.48550/arXiv.1908.03851.

[47] Müller, D., Soto-Rey, I. & Kramer, F. Towards a guideline for evaluation metrics in medical image segmentation. BMC Res Notes 15, 210 (2022). https://doi.org/10.1186/s13104-022-06096-y.

[48] Thangavel, K., Sasirekha, K. (2022). Classification of COVID-19 Chest CT Images Using Optimized Deep Convolutional Generative Adversarial Network and Deep CNN. In: Saras-wat, M., Sharma, H., Balachandran, K., Kim, J.H., Bansal, J.C. (eds) Congress on Intelligent Systems. Lecture Notes on Data Engineering and Communications Technologies, vol 111. Springer, Singapore. https://doi.org/10.1007/978-981-16-9113-3_27.

[49] Sasirekha, K. and Thangavel, K. Biometric face classification with the hybridized rough neural network, International Journal of Biometrics, volume 12, 2020, https://doi.org/ 10.1504/IJBM.2020.107717.